J. Fluid Mech. (1987), *vol.* 182, *pp.* 291–314
Printed in Great Britain

Experimental study of three shock wave/turbulent boundary layer interactions

By ALEXANDER J. SMITS AND KIN-CHOONG MUCK
Gas Dynamics Laboratory, Department of Mechanical and Aerospace Engineering, Princeton University, Princeton, NJ 08544, USA

(Received 17 June 1986 and in revised form 19 February 1987)

Experiments were performed to investigate the supersonic flow of a turbulent boundary layer over a number of compression-corner models. Upstream of each corner, the free-stream Mach number was 2.9 and the incoming boundary layer was typical of a two-dimensional, zero-pressure-gradient, high-Reynolds-number flow. Three different corner angles were used, namely 8°, 16° and 20°, and at the highest angle the interaction was strong enough to cause separation. Each flow was investigated using normal and inclined hot wires, and measurements of the longitudinal mass-flux fluctuations and the mass-weighted turbulent shear stress are presented. The behaviour of the kinematic and Reynolds stresses, deduced from the mass-weighted quantities by applying Morkovin's 'strong Reynolds analogy', is also considered. In all three flow cases, the interaction dramatically amplifies the turbulent stresses, and the amplification increases with increasing turning angle. Different stress components are amplified by different amounts, however, and the structure parameter $-\overline{u'v'}/\overline{u'^2}$ changes significantly through the interaction. Perhaps more importantly, the nature of these changes depends on the strength of the interaction. This result is rather unexpected, and it is believed to be due mainly to the unsteadiness of the shock system. It is suggested that the apparently random motion of the shock system affects the normal stresses more than the shearing stresses, and, since the unsteadiness increases with corner angle, the effect on the turbulence structure also becomes more pronounced.

1. Introduction

When a turbulent boundary layer encounters a compression corner, a system of compression waves forms in the supersonic part of the flow, and the resulting flow field is the product of a complicated interaction between this shock system and the incoming boundary layer. Within the interaction, large gradients in static pressure, skin friction and mass-flow rate occur, and if the turning angle is large enough the flow separates and becomes unsteady owing to shock oscillation (Settles, Fitzpatrick & Bogdonoff 1979; Dolling & Murphy 1982). These shock wave/boundary layer interactions are of great practical importance, and therefore they have been extensively studied in the past (see, for example, Green 1970; Adamson & Messiter 1980; Agrawal & Messiter 1984). Despite this attention, they are not well understood, primarily because we lack information regarding the turbulence behaviour. Existing turbulence measurements are scarce and often of dubious quality (Fernholz & Finley 1981) and as a result turbulence modelling for shock wave/boundary layer interactions continues to be rather primitive. Computations tend to rely on conventional turbulence models which are inherently incapable of dealing with the

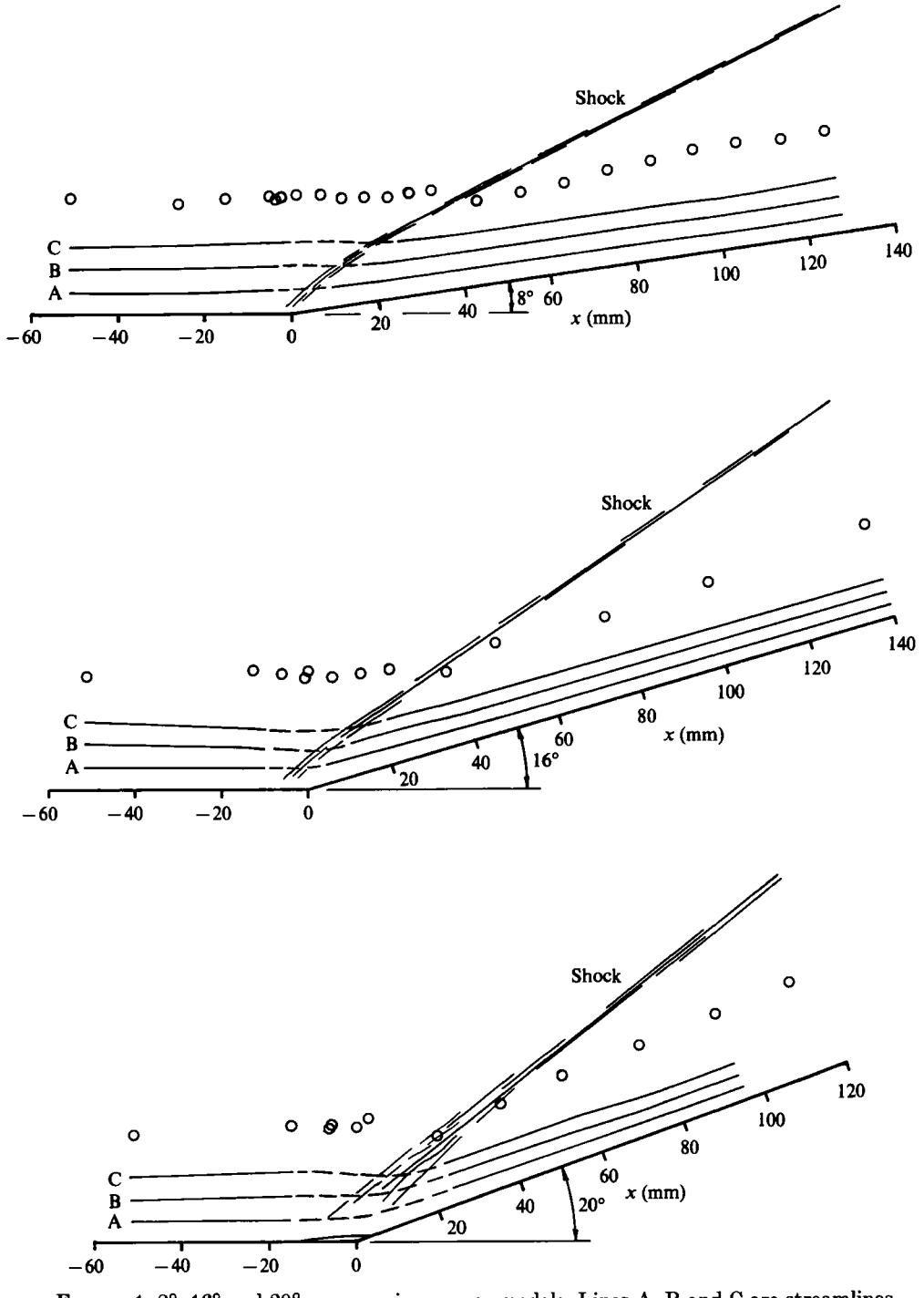

FIGURE 1. 8°, 16° and 20° compression-corner models. Lines A, B and C are streamlines originating at $y/\delta_0 = 0.2$, and 0.4 and 0.6 respectively; ○, boundary-layer thickness.

sudden and severe perturbations encountered in the interaction zone. Not surprisingly, the computations have therefore met with little success, particularly at higher corner angles (see for instance Horstman *et al.* 1977; Coakley, Viegas & Horstman 1977; Visbal & Knight 1983).

The present experiments were designed to improve our understanding of the turbulence behaviour in these flows. They represent a systematic study of two-dimensional compression-corner flows, covering a range of shock strengths. The wind tunnel and compression-corner models used in this investigation were identical with those used by Settles *et al.* (1979) in a study of the mean-flow behaviour (see figure 1). The measurements by Settles *et al.* were subsequently adopted as a test case by the 1980–81 Stanford conference (Kline, Cantwell & Lilley 1981). Hence, the turbulence measurements, in addition to improving our fundamental understanding of turbulence behaviour, provide valuable information for testing calculation methods. To facilitate future work, the turbulence data have been compiled in standard form (Muck, Hayakawa & Smits 1983*a*, *b*; Muck, Spina & Smits 1984), and these reports are available on request from the authors.

To measure the turbulence, constant-temperature hot-wire anemometry was used. Normal- and inclined-wire surveys were made and the measurements show the behaviour of the longitudinal mass-flux fluctuations $\langle(\rho u)'\rangle$ and the mass-weighted shear stress $\overline{(\rho u)'v'}$. To gain further insight into the turbulence structure, the Reynolds stresses $\overline{\rho u'^2}$ and $\overline{\rho u'v'}$ were deduced using the 'strong Reynolds analogy' suggested by Morkovin (1962). Throughout this paper, the velocity components in the x- and y-directions, that is, the components parallel and normal to the wall, are denoted by u and v, respectively. Primes indicate fluctuating quantities, overbars represent time averages, and the symbol $\langle\ \rangle$ is used to denote r.m.s. values.

This paper is the last in a series reporting the turbulence behaviour in shock wave/boundary layer interactions (see Hayakawa *et al.* 1983; Hayakawa, Smits & Bogdonoff 1984*a* and Muck & Smits 1984*a*, *b*). In the present contribution, additional results are presented but, more importantly, the results are examined in an overall sense, and our principal concern is to investigate connections among the separate experiments and to determine the common mechanisms at work.

A preliminary discussion is given in §2. The apparatus and experimental techniques are described briefly in §3, and in §4 we present the results. These results are discussed in §5 and the conclusions are given in §6.

2. Preliminary discussion

By way of introduction to the overall behaviour, consider the shadowgraphs of the instantaneous flow fields shown in figure 2 (note that the curved boundaries on the left and right of the pictures are part of the perimeter of the circular window, not part of the model). Qualitatively, the turbulent mixing appears to be considerably enhanced across the shock and the trend is more pronounced as the shock strength increases. The incursions of free-stream fluid appear to become much deeper, suggesting that the lengthscales of the turbulent motions have correspondingly increased. At the smallest corner angle, the shock remains quite distinct almost to the surface but as the corner angle increases the shock appears to fan out and break out into a system of compression waves. Shadowgraphs, however, represent a spatial average across the flow and do not give a good indication of the behaviour in any given streamwise plane. Muck, Dussauge & Bogdonoff (1985) demonstrated that the

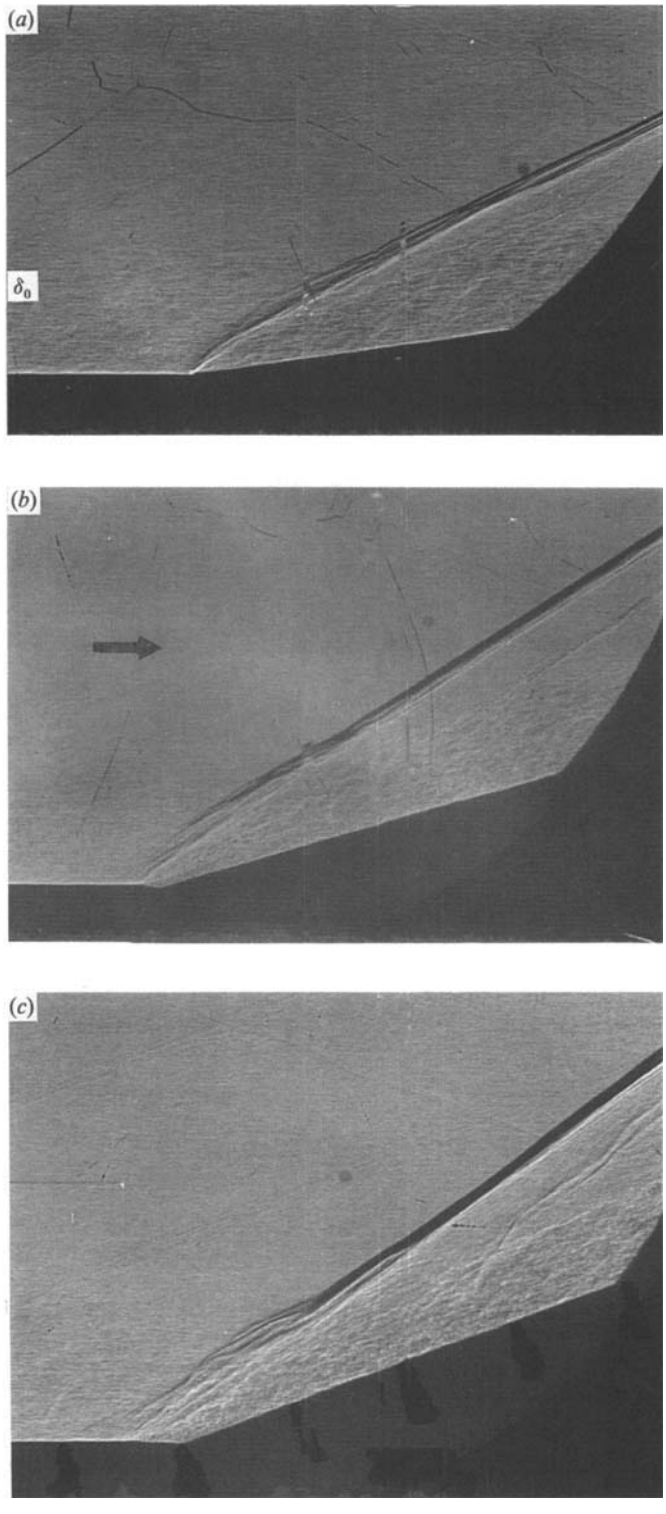

FIGURE 2. Flow-field shadowgraphs. Flow is left to right (*a*) 8° corner, (*b*) 16°, (*c*) 20° (photographs provided by G. S. Settles).

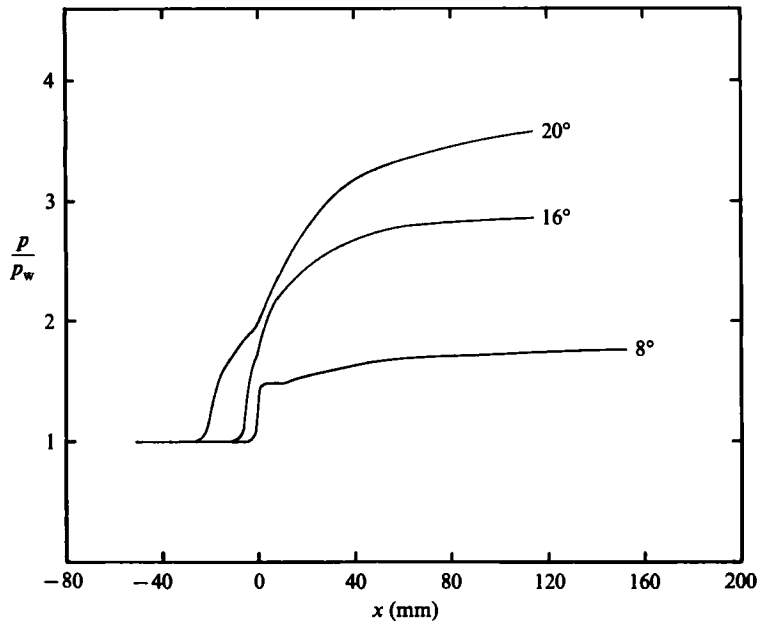

FIGURE 3. Wall-pressure distributions. The lines are faired through the experimental data of Settles *et al.* (1979). The pressure is non-dimensionalized by the static pressure upstream of the corner.

shock front is wrinkled in the spanwise direction, and the shock does not appear to split. In addition, Dolling & Murphy (1982) found that the shock sheet exhibits significant streamwise flapping, introducing large fluctuations in the instantaneous pressure field at points ahead of the corner, thereby causing the mean pressure to rise. This 'upstream influence' is seen in the wall-pressure distributions (figure 3) and it increases with corner angle, indicating that the unsteadiness of the shock system becomes more important as the shock strength increases. Figure 3 also indicates that only part of the total compression and turning occurs across the wave system, and compression and streamline curvature continue for several boundary-layer thicknesses downstream of the corner.

The skin-friction coefficients (figure 4) indicate a sudden decrease in wall shear in the interaction zone. Both the 16° and 20° corners exhibit regions of separated flow, and the position of the mean separation and reattachment lines agree well with the results of the surface flow visualization (Settles *et al.* 1979). The separated zone for the 16° corner is very small, however, and the flow is more accurately described as representing 'incipient separation'. Downstream of reattachment, the wall shear quickly recovers and continues to rise, and eventually it overshoots the self-preserving level.

The flow patterns demonstrated the overall two-dimensionality of the flow for the 8° and 16° models, and only minor convergence and divergence effects were observed. For the 20° corner, some small, almost periodic wiggles were seen in the separation and reattachment lines, and the surface streaks displayed a cellular character in the separated zone. These spanwise variations were much more apparent for the 24° corner, the highest corner angle tested by Settles *et al.*, and may indicate the presence of longitudinal roll cells such as those observed in concavely curved shear layers. Similar surface flow patterns were observed near reattachment by Roshko & Thomke

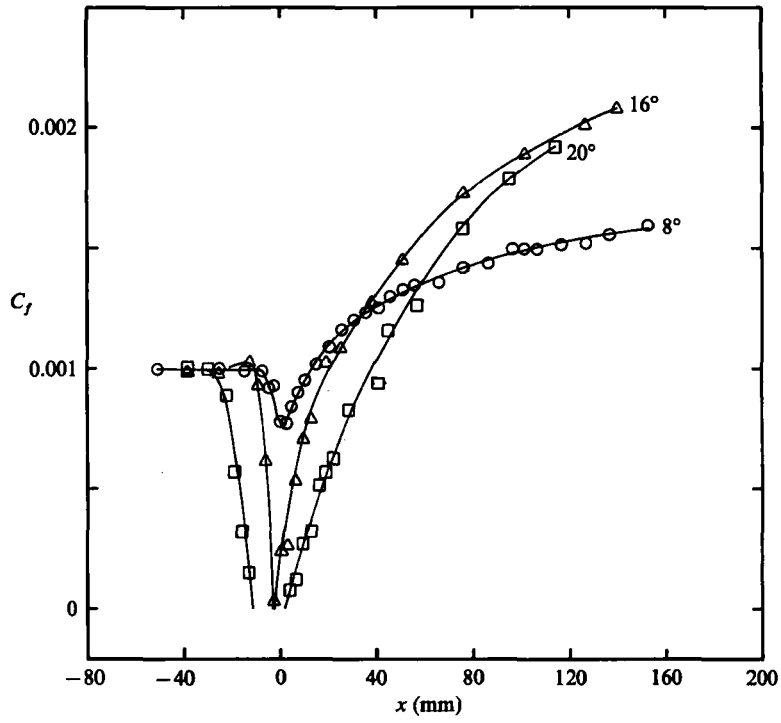

FIGURE 4. Preston tube skin-friction distributions, indicating incipient separation for the 16° corner (from Settles *et al.* 1979). The wall stress was non-dimensionalized using 'effective' density and local boundary-layer edge velocity based on tunnel stagnation and local static pressures.

(1966) and Shamroth & MacDonald (1970), and they seem to be a general feature of supersonic, separated flows. In contrast, longitudinal vortices do not seem to be a regular feature in subsonic step cases. In the supersonic case, however, strong compressibility effects are present in addition to concave-curvature effects, and it is possible that a nonlinear coupling occurs to generate organized, longitudinal vorticity. The current experiments are restricted to a maximum corner angle of 20° where these three-dimensional effects are probably small.

The mean-velocity profiles, scaled according to the van Driest transformation (figure 5), provide further evidence for an increase in turbulence scale. The velocity data of Settles *et al.* were re-analysed with the underlying assumption that the inner layer is quick to adjust to any perturbation (see, for example, Smits & Wood 1985), and therefore a fit of the near-wall data to the standard log-law was assumed to give a good estimate for the wall stress. This argument can also be used to show that the Van Driest transformation should hold to a reasonable approximation in the near-wall region, despite the strong perturbations experienced by the flow. All the profiles downstream of the shock show a characteristic 'dip' below the log-law. A similar behaviour was found by Smits, Young & Bradshaw (1979*b*), and Taylor & Smits (1984) in subsonic and supersonic flows downstream of a short region of concave curvature, and by Smits, Eaton & Bradshaw (1979*a*) in subsonic flows with lateral divergence and concave curvature. These dips suggest that in this region the lengthscale increases with distance from the wall at a rate greater than Ky, where K is the von Kármán constant and y is the distance from the wall.

As far as the turbulence behaviour is concerned, the earlier studies by Rose (1973)

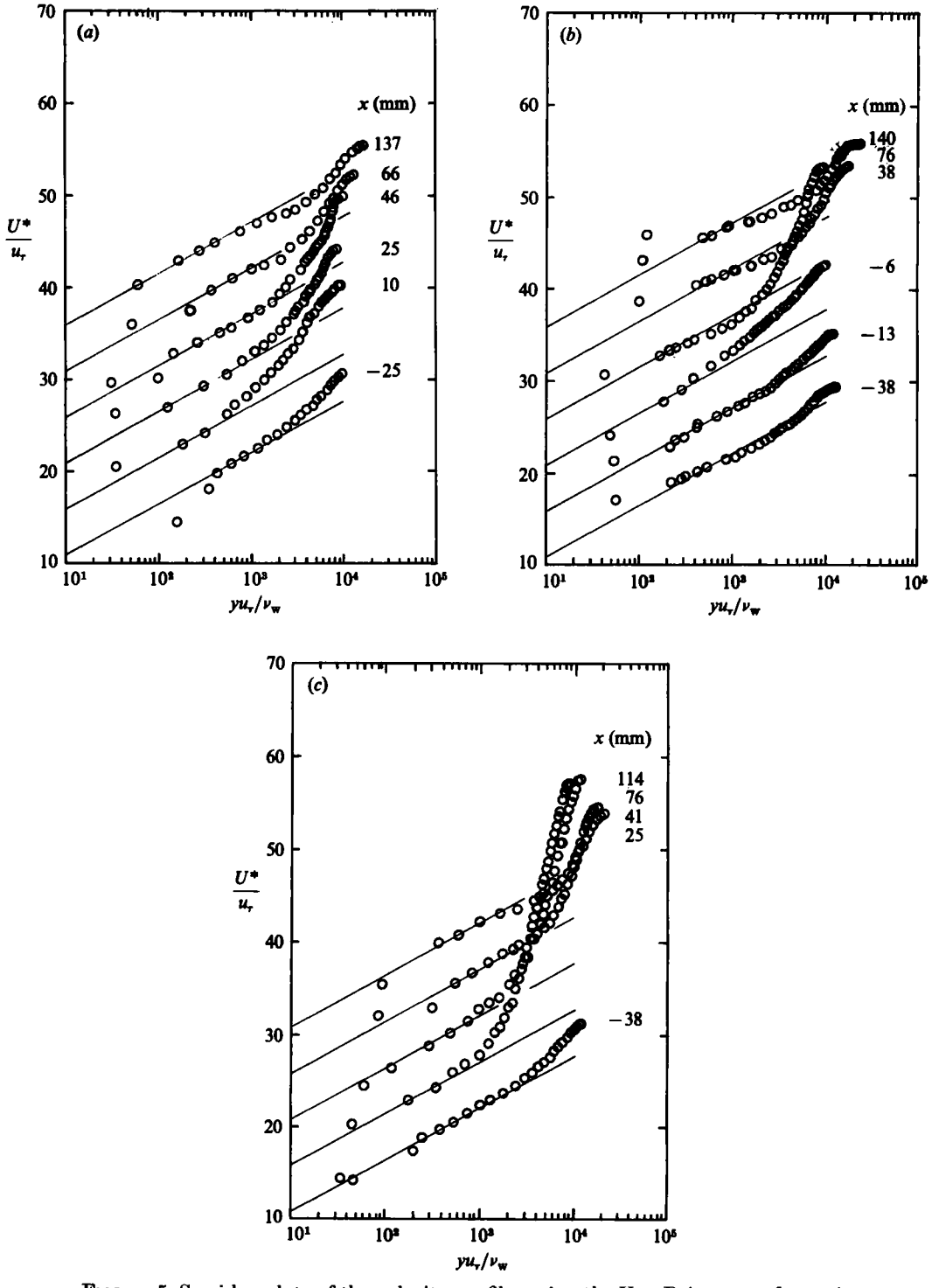

FIGURE 5. Semi-log plots of the velocity profiles using the Van Driest transformation: (*a*) 8° corner, (*b*) 16°, (*c*) 20°.

and Kussoy & Horstman (1975) of shock wave/boundary layer interactions on a flat plate indicated that the turbulence levels in the interaction were strongly amplified, a result that may have been anticipated from the shadowgraphs shown in figure 2. Rose presented the first shear-stress measurements ever taken in an interaction, and observed dramatic increases through the interaction. Unfortunately, the layer was very thin and the accuracy of the data is probably questionable. Nevertheless, these results, and those by Kussoy & Horstman, provided the first direct evidence for the powerful turbulence amplification experienced in shock wave/boundary layer interactions.

For the compression-corner geometry, Ardonceau *et al.* (1979) used hot-wire and laser-Doppler anemometry to investigate the turbulence behaviour for three turning angles at Mach 2.25. The flow was separated at the highest corner angle. No shear-stress results were reported, but the data included measurements of $\langle(\rho u)'\rangle$, $\langle u'\rangle$ and $\langle v'\rangle$. A large turbulence amplification was observed, particularly for the longitudinal component. The anisotropy ratio $\langle u'\rangle/\langle v'\rangle$ displayed a very sharp increase also, particularly for the separated-flow case, and Ardonceau *et al.* suggested that this was caused by the slow action of the pressure–strain correlations in distributing the turbulent kinetic energy from the longitudinal component, where it is produced, to the other components. The anisotropy parameter relaxed rather quickly, however, and at six initial boundary-layer thicknesses downstream of the corner had recovered to about its upstream value.

Despite this earlier work, a number of questions remain. No attempt has been made to distinguish among the effects of the shock wave, compression and curvature on the turbulence, and the non-equilibrium nature of the turbulence response is not well understood. The unsteadiness at higher shock strengths has received little experimental attention, and quantitative evidence regarding the behaviour of the length-scales is very scarce. The current paper attempts to provide further information that will contribute towards answering these questions.

3. Apparatus and techniques

The wind tunnel, compression-corner models and experimental techniques are described by Hayakawa *et al.* (1984*a*), and Muck & Smits (1984*b*), and therefore only the most pertinent information will be presented here.

The tunnel was a 203 mm × 203 mm blowdown facility, with fixed nozzle blocks. Each model was mounted on the floor of the tunnel at the same distance downstream of the nozzle throat, and the stagnation conditions (see table 1) were similar for all tests. The models were simple ramps, 152 mm wide, and they were fitted with aerodynamic fences to minimize three-dimensional effects. The incoming boundary layer developed on the nearly adiabatic tunnel wall experienced a natural transition, and was typical of a zero-pressure-gradient, two-dimensional, high-Reynolds-number turbulent boundary layer. Just prior to each interaction, the layer had a thickness of approximately 26 mm, and a Reynolds number based on momentum thickness of about 78000.

Constant-temperature hot-wire anemometry was used throughout. A detailed description of the calibration and measurement techniques is given by Smits, Muck & Hayakawa (1983) and Smits & Muck (1984). Briefly, the wires were connected to DISA 55M10 anemometers, and operated at overheat ratios of 1.1 or higher. At these high overheats, the output of the anemometer is primarily sensitive to mass-flow fluctuations, and therefore the contributions from total-temperature fluctuations

α	8°	16°	20°
Re_{ref}/m	6.3×10^7/m	6.3×10^7/m	6.3×10^7/m
M_{ref}	2.87	2.85	2.79
p_0	6.9×10^5 Nt/m^2	6.9×10^5 Nt/m^2	6.9×10^5 Nt/m^2
p_w	2.3×10^4 Nt/m^2	2.4×10^4 Nt/m^2	2.6×10^4 Nt/m^2
T_w/T_0	1.04	1.04	1.04
T_0	260 K	252 K	263 K
U_{ref}	571 m/s	576 m/s	562 m/s
δ_{ref}	26.0 mm	26.0 mm	25.0 mm

TABLE 1. Incoming flow parameters taken at $x = -50.8$ mm

were neglected. Normal wires were used to measure the mass-flux fluctuations. Inclined wires were used to measure the mass-weighted shear stress $\overline{(\rho u)'v'}$ by performing two surveys, where the second survey was performed with the wire rotated 180° about the probe axis relative to the first. The misalignment on rotation was always less than 1°.

Two aspects of the data deserve further attention. First, the analog-to-digital converter had a maximum conversion speed of 500 kHz, and a maximum record length of 1024 points, corresponding to an effective frequency band of approximately 400 Hz–250 kHz. To measure the turbulence intensities, 25 records of 1024 points each were taken, resulting in a convergence uncertainty of less than 1%. For the time-series analyses, two records were taken at a given point with conversion rates of 25 kHz and 500 kHz. By combining these data, frequencies from 20 Hz–250 kHz could be resolved. However, the upper limit on the frequency resolution is set by the spatial resolution of the hot-wire probe and the limited frequency response of the anemometer. These limits combine to fix the upper frequency response of the system at approximately 120 kHz.

The second aspect to consider is that the calibration was performed at a fixed Mach number, equal to the free-stream value. Kovasznay (1950) showed that the hot-wire response is independent of Mach number, as long as the Mach number normal to the wire filament exceeds 1.2. In addition, Horstman & Rose (1975) and Rose & McDaid (1979) showed that at a sufficiently high Reynolds number and overheat ratio, the mass-flow-rate sensitivity of a normal wire is virtually independent of Mach number. Recent work by Rong, Tan & Smits (1985) confirms that Mach-number effects for the normal-wire results presented here are negligible at any distance from the wall. For the inclined-wire surveys, however, the sensitivity to v' in the transonic regime is a strong function of the normal Mach number, and therefore the shear-stress results are only valid in regions where the normal Mach number exceeds 1.2. This restriction severely limits the accuracy of the measurements near the wall, and, to reduce this source of error, wire angles of about 30° were used instead of the more conventional 45° to increase the normal Mach number at a given distance from the wall.

Overall accuracies were determined from an error analysis to take account of both systematic and random errors. In the upstream boundary layer at the mid-point, the uncertainty in $\langle(\rho u)'\rangle$ was estimated to be -5% to $+9\%$ (systematic uncertainty $+2\%$), and the corresponding uncertainty in $\overline{(\rho u)'v'}$ was about -27% to $+11\%$ (systematic uncertainty -8%), as long as the normal-Mach-number criterion was satisfied. The data for the transverse component of the normal stress $\overline{v'^2}$ suffered from an accumulation of errors and they were discarded.

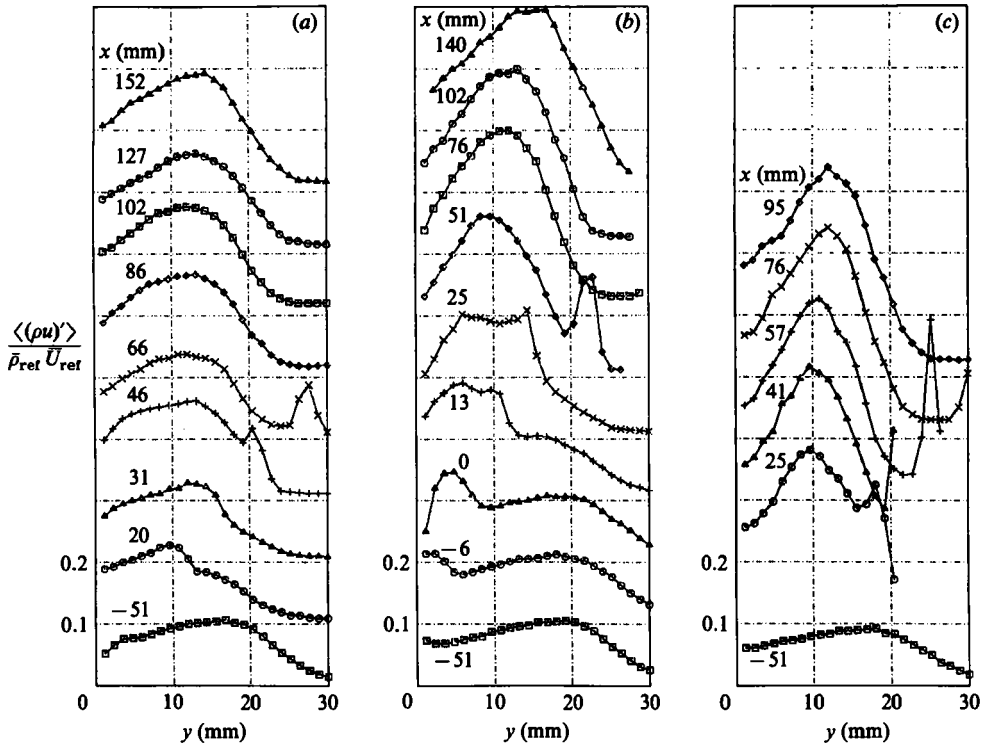

FIGURE 6. Mass-flux fluctuation profiles for the compression corners: (*a*) 8°, (*b*) 16°, (*c*) 20°.

Total-temperature fluctuations were not measured. To deduce the kinematic stress $\overline{u'^2}$, and the Reynolds stresses $\bar{\rho}\overline{u'^2}$ and $\bar{\rho}\overline{u'v'}$ from the mass-weighted quantities $\overline{(\rho u)'^2}$ and $\overline{(\rho u)'v'}$, Morkovin's (1962) 'strong Reynolds analogy' was assumed; that is, pressure fluctuations and total-temperature fluctuations were assumed to be small. Hence, the density and velocity fluctuations were assumed to be related according to

$$\frac{\langle \rho' \rangle}{\bar{\rho}} = (\gamma - 1)\, Ma^2 \frac{\langle u' \rangle}{\bar{U}},$$

where Ma is the local Mach number.

The measurements by Dussauge & Gaviglio (1981) in a boundary layer subjected to a rapid expansion provide strong support for these assumptions; they found that the correlation coefficient between density and longitudinal velocity fluctuations was nearly constant across the layer and equal to about 0.8, even for this severely perturbed boundary layer. The value of 0.8 was therefore used in all data reduction.

4. Results

The behaviour of the turbulent stresses is shown in figures 6–9. In rapidly changing flows, it is difficult to choose non-dimensionalizing variables that are meaningful, and therefore the incoming flow was used to define the reference parameters for the present results. The figures, therefore, indicate the behaviour of the absolute turbulence levels. The x- and y-coordinates were aligned with the local surface, and the hot-wire probes were aligned parallel to the local surface. In the region near the

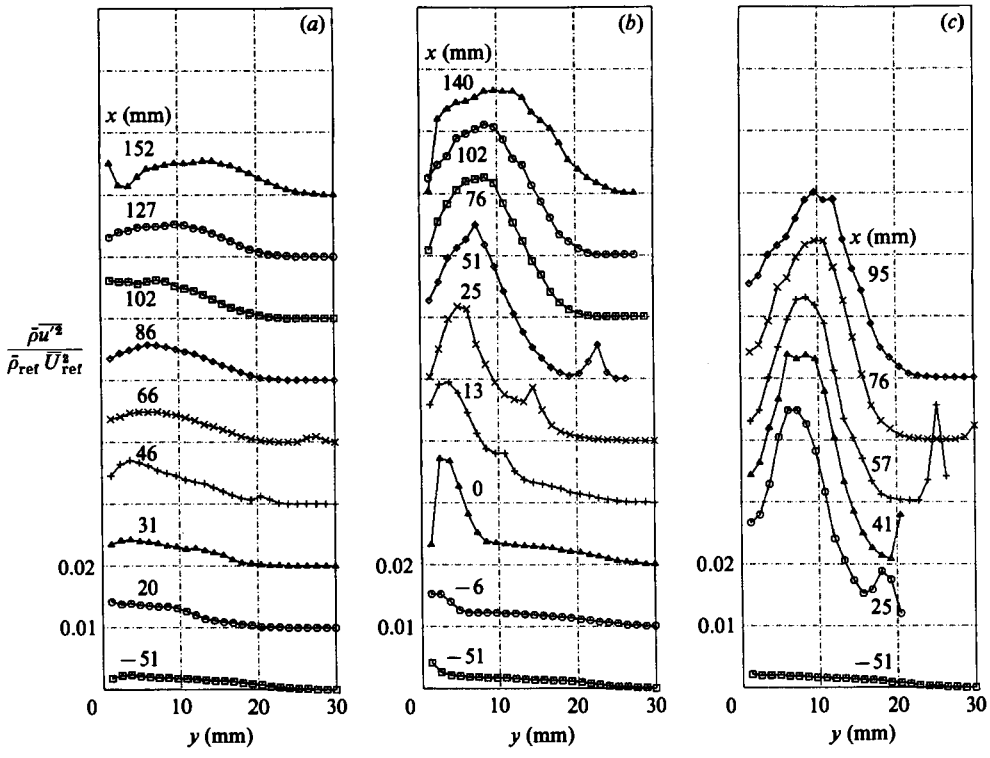

FIGURE 7. Longitudinal Reynolds-stress profiles for the compression corners: (*a*) 8°, (*b*) 16°, (*c*) 20°.

corner, the direction of the mean local flow does not generally coincide with the direction of the x-coordinate. The normal wire measures the mass-flux intensity in the direction normal to the wire, and therefore the results for $\langle(\rho u)'\rangle$ and $\overline{\rho u'^2}$ are insensitive to a change in free-stream direction. However, the inclined wire measures $\overline{(\rho u)'v'}$ in coordinates aligned with the probe, and when the flow direction changes significantly within a profile the accuracy of $\overline{(\rho u)'v'}$ is affected strongly. For the downstream profiles, therefore, only the measurements downstream of the shock are reliable.

The results confirm that the interactions produce a large increase in turbulence activity. The mass-flux fluctuation intensity, for example, increases by four to fifteen times (figure 6), and the amplification of the mass-weighted shear stress is even greater. Where the shock wave passes through the profile, the unsteady shock motion smears the region over which the amplification occurs, and it sometimes produces a local peak in the intensity profiles. The results given in figure 9 show this behaviour clearly. It appears that the region directly affected by the shock has a thickness of about 0.1δ for the 8° case, and 0.2δ for the 16° case. Dolling & Or (1983) measured the extent of the unsteady shock motion at the wall, and found that it measured approximately 0.15δ and 0.3δ for these two cases, respectively (see also figure 10). Clearly, the shock motion extends throughout the layer, and the amplitude of the motion is approximately constant with distance from the wall.

The amplification of the longitudinal Reynolds stress $\overline{\rho u'^2}$ follows a similar trend to that observed for the mass-flux fluctuation intensity (figure 7). In fact, the

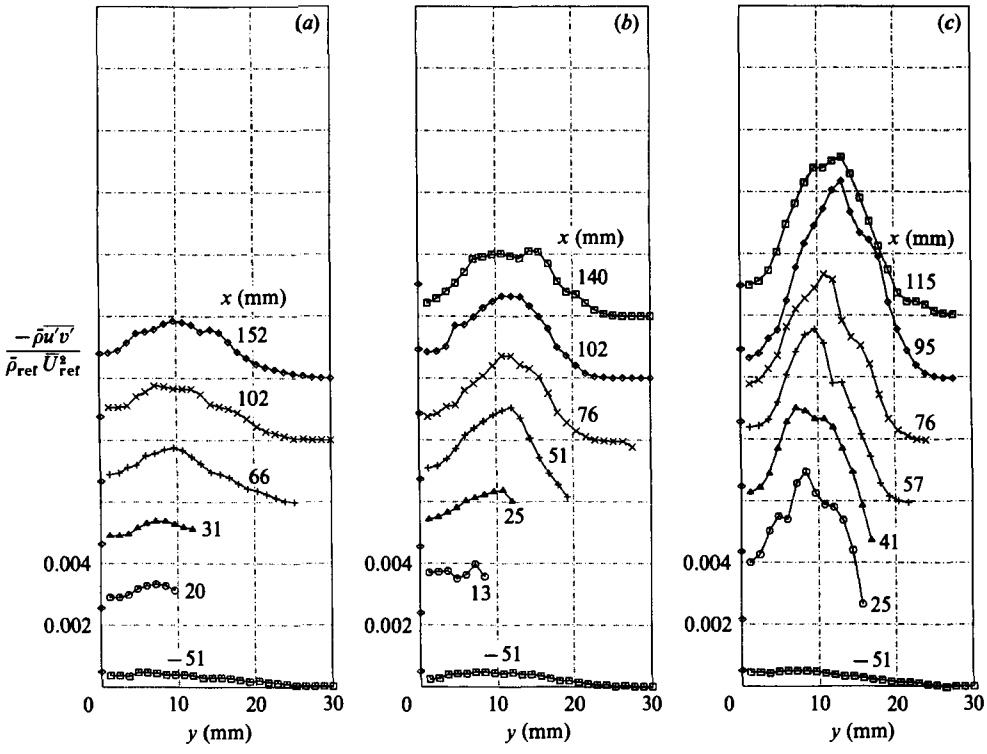

FIGURE 8. Reynolds-shear-stress profiles for the compression corners: (*a*) 8°, (*b*) 16°, (*c*) 20°.

experimental results, when taken together with the 'strong Reynolds analogy', indicate that the amplification of $\langle u' \rangle$ and $\langle \rho' \rangle$ is approximately equal to the amplification of $\langle (\rho u)' \rangle$ right across the layer.

To understand this amplification more fully, consider the evolution of the velocity turbulence intensity along different streamlines. Three streamlines, passing through the upstream boundary layer at the locations corresponding to $y/\delta_0 = 0.2$, 0.4 and 0.6 were selected for this purpose, and the results are given in figure 10. For comparison, the variation in the intensity of the wall-pressure fluctuation level is also shown. The rate of the response of $\overline{u'^2}$ is clearly a function of the distance from the wall. As expected, the eddies in the outer part of the layer respond more slowly to the amplification than the motions near the wall. The effect of dissipation is also felt more quickly near the wall, and, combined with the redistribution of $\overline{u'^2}$ among the other components, it causes a more rapid attenuation of the turbulence activity there.

Figures 7 and 8 indicate that the behaviour of the Reynolds stresses $\bar{\rho}\overline{u'^2}$ and $\bar{\rho}\overline{u'v'}$ are qualitatively very similar. Quantitatively, however, their relative amplification is different, suggesting that the turbulence structure changes through the interaction. For instance, the ratio $a'' = -\overline{u'v'}/\overline{u'^2}$ can be taken as a structure parameter. In the undisturbed boundary layer at $x = 51$ mm, this ratio has a value of about 0.25 (at $y/\delta_0 = 0.6$), which agrees well with the value commonly quoted for incompressible boundary layers (see, for example, Townsend 1976). For the 8° corner, a'' increases to about 0.45 through the shock (see figure 11) and displays little attenuation further downstream. For the 16° corner, however, a'' decreases sharply near the wall

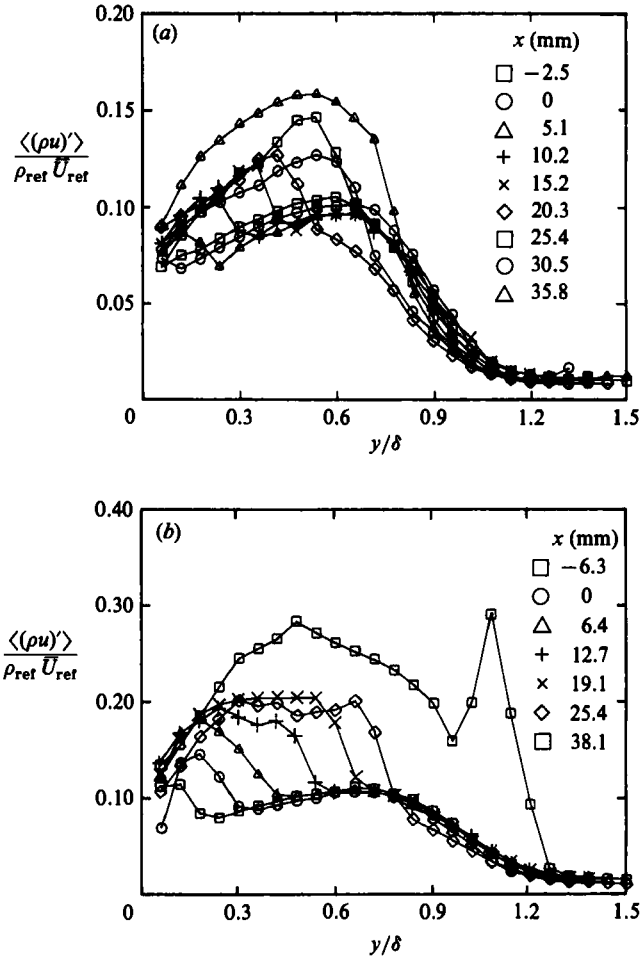

FIGURE 9. Profiles of root-mean-square mass-flux intensity for the region close to the corner: (*a*) 8° corner, (*b*) 16°.

($y < 5$ mm), and near the centre of the layer ($y \approx 10$–12 mm) it first increases before rapidly decreasing. The 20° results differ again; in passing through the shock, a'' decreases significantly near the wall but increases in the centre of the layer. The higher values near the centre of the layer show little attenuation but the measurements do not extend as far downstream as in the other two cases, and the subsequent relaxation behaviour is unknown. The behaviour of a'' is further considered in §5.

The mixing lengths were calculated using the measured shear stress and velocity profiles. The profiles shown in figure 12 display considerable scatter especially in the outer layer (associated with the uncertainties in measuring $\bar{\rho}\overline{u'v'}$ and the difficulties encountered in the differentiation of discrete data). Nevertheless, the values in the undisturbed boundary layer agree well with the generally accepted incompressible distribution, and near the wall some trends can be discerned. It appears that the mixing length for $y/\delta_0 < 0.4$ is initially reduced but eventually increases to larger than normal values. The results partially confirm the earlier observations from the velocity profiles that the lengthscales near the wall increase with distance from the

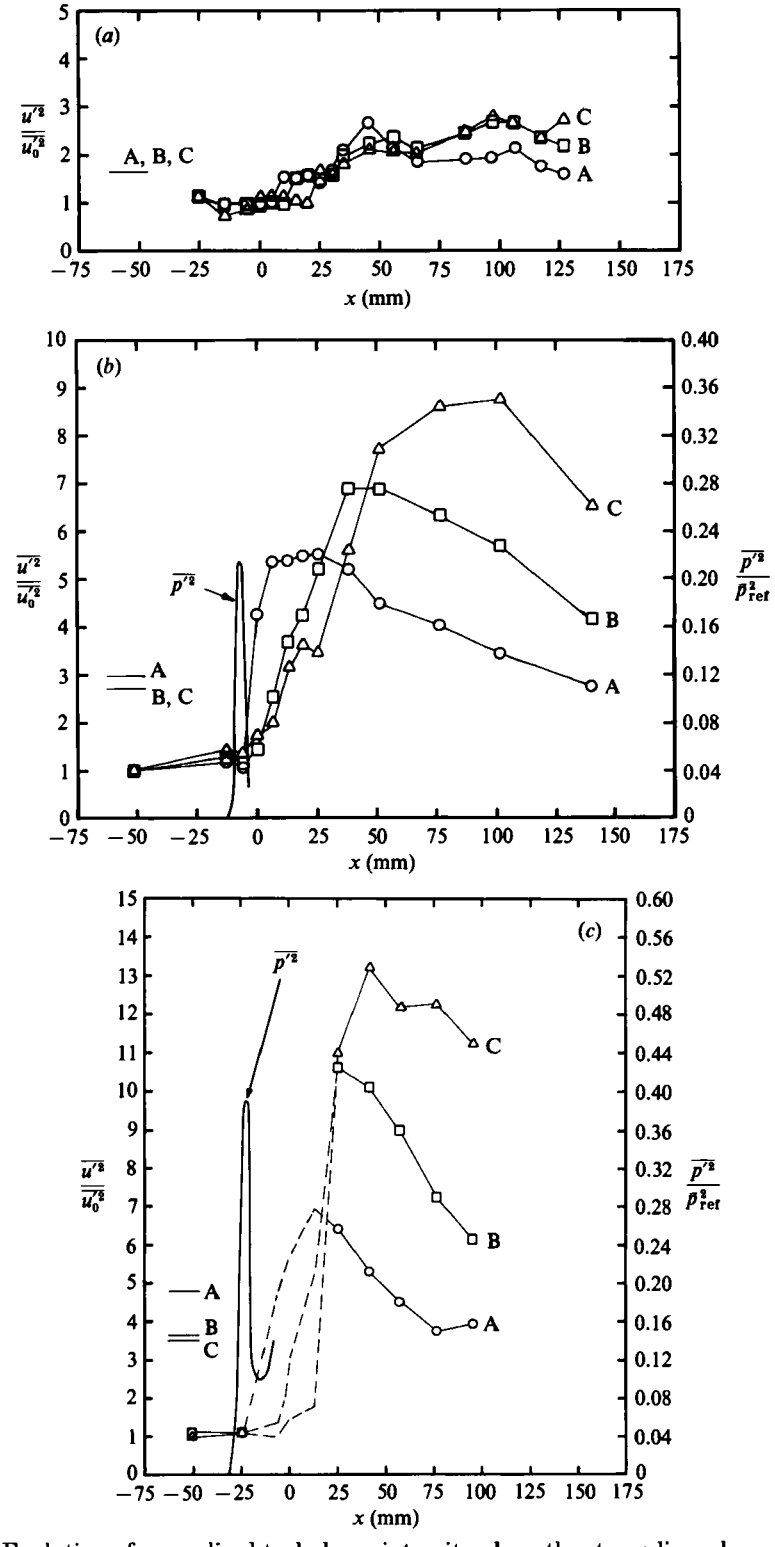

FIGURE 10. Evolution of normalized turbulence intensity along the streamlines shown in figure 1: (*a*) 8° corner flow, (*b*) 16°, (*c*) 20°. Also shown are the wall-pressure fluctuation intensity distributions (from Dolling & Or 1983). Predictions from the analysis by Debieve *et al.* (1982) are shown on the left for the streamlines A, B and C.

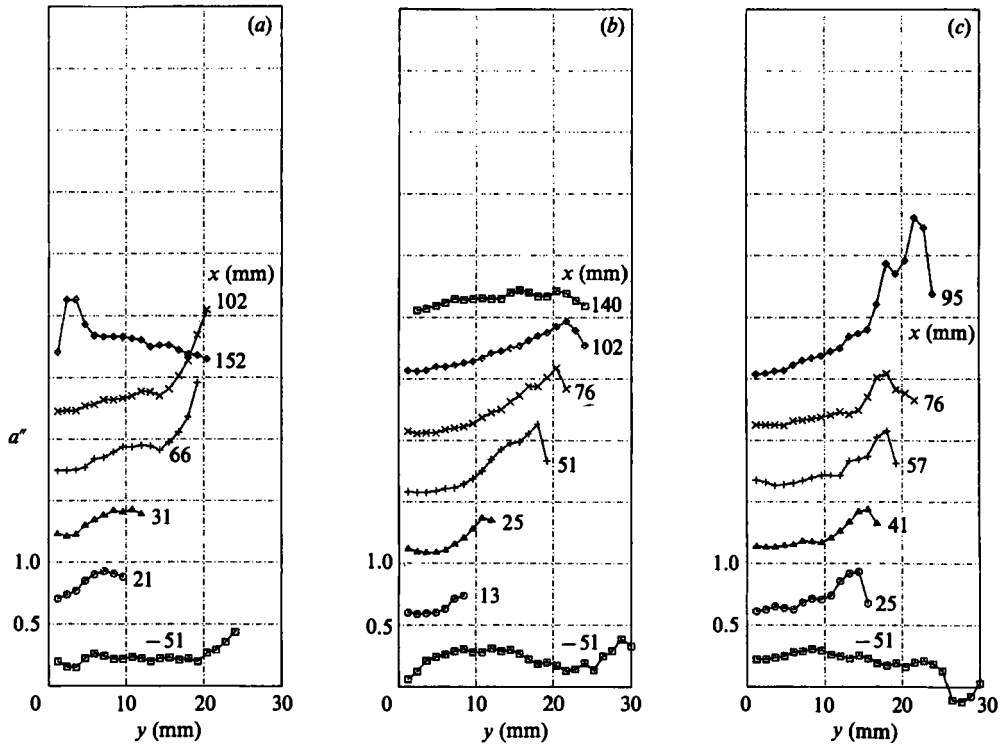

FIGURE 11. Profiles of the stress ratio $a'' = -\overline{u'v'}/\overline{u'^2}$; (*a*) 8° corner, (*b*) 16°, (*c*) 20°.

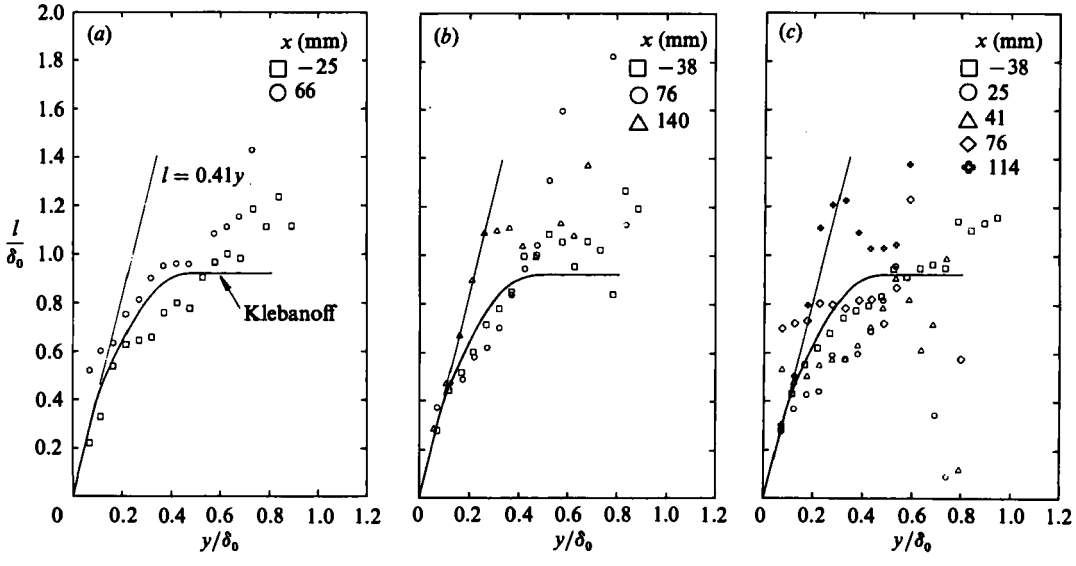

FIGURE 12. Profiles of mixing length: (*a*) 8° corner, (*b*) 16°, (*c*) 20°.

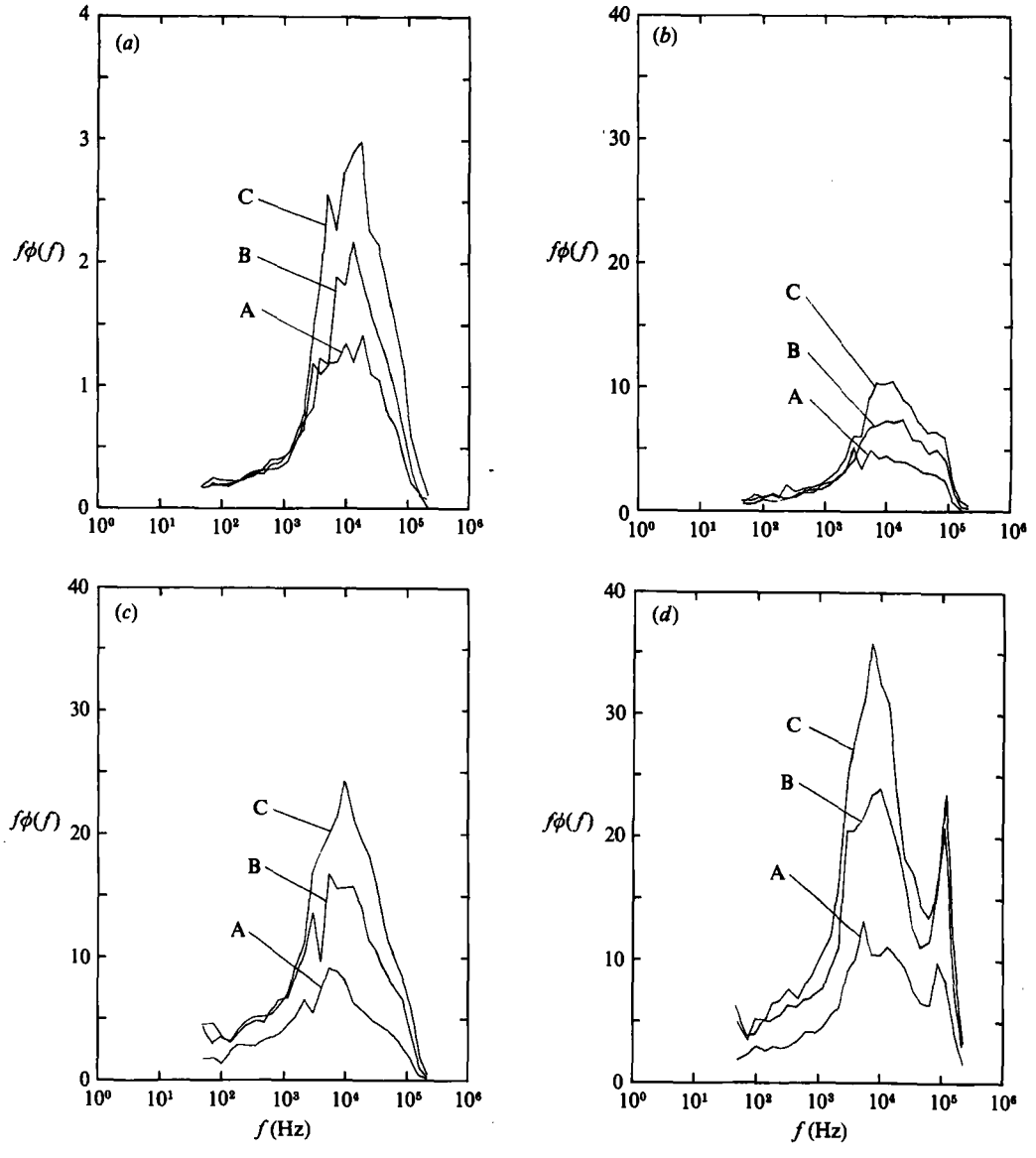

FIGURE 13. Energy spectra of the longitudinal mass-flux fluctuations. (*a*) Incoming boundary layer, $x = 51$ mm; (*b*) 8° corner, $x = 102$ mm; (*c*) 16°, $x = 152$ mm; (*d*) 20°, $x = 95$ mm. The positions within the boundary layer correspond to the streamlines shown in figure 1.

wall at a rate greater than Ky. The scatter in the data prevents further analysis. It seems, however, that the change in the mixing length is of the same order as that observed by Jayaram, Taylor & Smits (1987) in a series of nearly isentropic compressions.

To investigate the behaviour of the time and frequency scales, the energy spectra were calculated at certain points along streamlines in the flow. The streamlines were the same as those used to show the amplification of the turbulent velocity intensity $\overline{u'^2}$ in figure 10. The curves shown in figure 13 were smoothed over equal logarithmic increments in frequency. The area under each curve is directly proportional to $\overline{(\rho u)'^2}$,

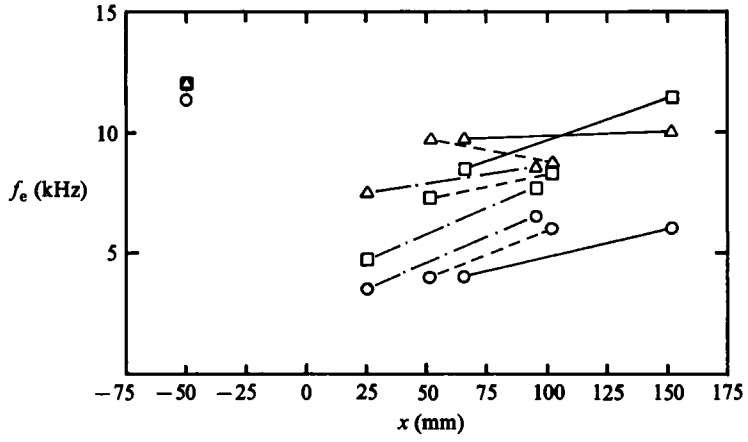

FIGURE 14. Variation of the peak in the energy spectrum along the streamlines shown in figure 1: ○, streamline A; □, B; △, C. Lines are shown for clarity only: ——, 8° corner; – – –, 16°; —·—, 20°.

and the peak corresponds to the frequency of the most energetic motions f_e. (According to the strong Reynolds analogy, the spectral content of u', ρ' and $(\rho u)'$ should be similar.) The spectra clearly show the amplification of the turbulence levels, as well as displaying a shift in energy content, especially near the wall. The shift in f_e is plotted as a function of streamwise distance in figure 14. The change in convection velocity is unknown. However, the change in the free-stream velocity is only small (for the 8°, 16° and 20° cases it decreases by 5.6%, 12.9% and 17.6% respectively), and the results imply that a large increase occurs in the scale of the turbulence, especially near the wall. The results are very similar to those obtained by Jayaram & Smits (1985) and Jayaram *et al.* (1987) in boundary layers flowing over smoothly curved concave walls.

In addition to the time-averaged properties of the turbulence, the statistical properties give some guide to the nature of the turbulence transport process (see figure 15). The normalized mass-flux probability distributions for the undisturbed boundary layer appear very much as they do in a corresponding subsonic flow (Hayakawa *et al.* 1984*a*). At $y/\delta_0 = 1.2$, the fluctuations arise entirely from the free-stream flow and the distribution is Gaussian. At $y/\delta_0 = 1.0$, the intermittent nature of the turbulence in the outer part of the boundary layer is clearly seen as negative one-sided peaks start to appear sporadically on the signal trace. As we move closer to the wall, progressively more spikes appear, causing a negatively skewed probability-density distribution. At $y/\delta_0 = 0.5$, the signal becomes almost symmetrical around the mean value, and the distribution is approximately Gaussian. Closer to the wall, the distribution becomes positively skewed and the skewness increases monotonically towards the wall.

In the 8° corner flow, the shape of the probability-density distribution changes little as the flow moves through the shock. Despite the sudden increase in the absolute magnitude of the mass-flux fluctuations, the only discernible change through the shock is a slight growth in the intermittent zone, and the dimensionless higher-order moments remain virtually constant (see also Hayakawa *et al.* 1984*a*).

As the shock strength increases, however, the increasing distortion of the turbulence begins to affect the shape of the probability-density distribution. For the 16° flow, the distributions in the lower half of the boundary layer become increasingly

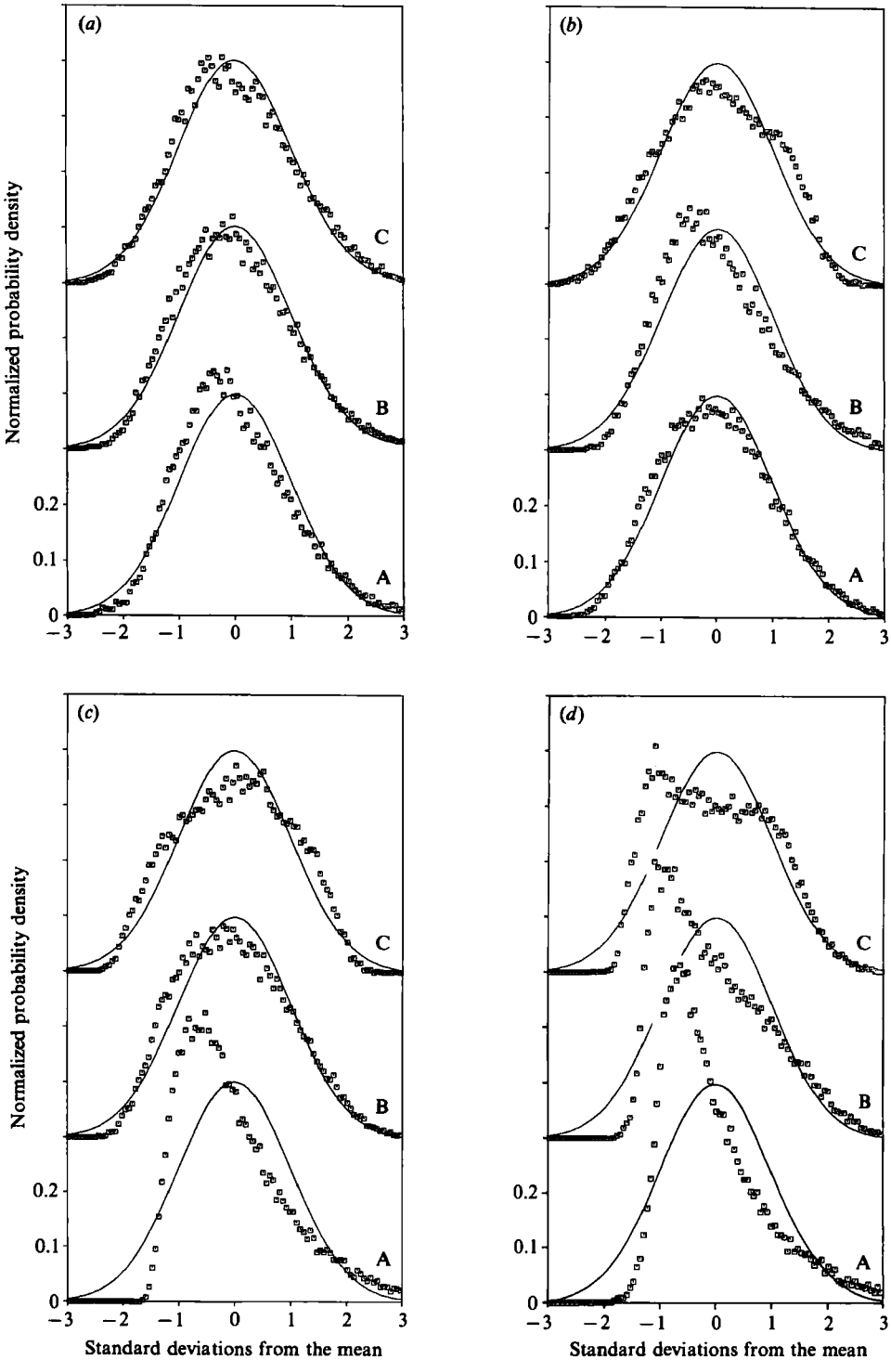

FIGURE 15. Probability-density distribution of the longitudinal mass-flux fluctuations. (*a*) Incoming boundary layer, $x = -51$ mm; (*b*) 8° corner, $x = 102$ mm; (*c*) 16°, $x = 152$ mm; (*d*) 20°, $x = 95$ mm. The positions within the boundary layer correspond to the streamlines shown in figure 1.

skewed, and this trend is even more apparent for the 20° flow. For $y/\delta_0 = 0.2$ and 0.4, the results indicate that the amplification of the turbulence intensity is largely due to an increase in the number of low-speed-fluid eruptions. These eruptions are still important at $y/\delta_0 = 0.6$, but at this point the incursions of free-stream fluid also become significant and the signal displays a strong intermittency, as is shown by the appearance of a second maximum in the probability-density distribution on the high-speed side. This strong contortion of the boundary-layer edge was anticipated from the shadowgraphs shown in figure 2.

5. Discussion

A number of mechanisms can be identified that are responsible for turbulence amplification in shock wave/boundary layer interactions. First, the turbulence level can increase dramatically in passing the shock wave as a consequence of the Rankine–Hugoniot jump conditions and the nonlinear coupling between the fluctuations in entropy, pressure and vorticity (Zang, Hussaini & Bushnell 1982; Anyiwo & Bushnell 1982; Debieve, Gouin & Gaviglio 1982). Secondly, the unsteady interaction between the moving shock and the turbulence is an effective mechanism for energy transfer, extracting energy from the mean flow and 'pumping' it into the turbulent motions (Hussaini, Collier & Bushnell 1985). Thirdly, downstream of the shock, the pressure continues to rise and the flow experiences further compression and concave streamline curvature. Both mechanisms are destabilizing and tend to increase turbulent activity (Bradshaw 1973, 1974).

It is difficult to discriminate quantitatively among these different influences. Nevertheless, some qualitative insight can be gained by adopting a number of simplifications. The interactions produce large density and pressure variations, and the forces due to pressure differences are much greater than the forces due to turbulent-stress gradients. For example, if Δp and τ_m are respectively the pressure increase and the maximum turbulent shear stress, then the ratio $(\Delta p)/\tau_m$ exceeds 20 for all three corner angles. If it is now assumed that the turbulent-kinetic-energy equation can be applied across a shock wave, and that the usual boundary-layer approximations apply, then the analyses given by Bradshaw (1974) and Dussauge & Gaviglio (1981) can be applied to shock wave/boundary layer interactions. In particular, if the effects of compression dominate,

$$\left(\frac{\overline{u_i u_j}}{\bar{\rho}}\right)^r = \text{const}$$

along a streamline, where r is an exponent whose value depends on the assumptions used. For example, Dussauge & Gaviglio neglected the contribution of the pressure-gradient terms to the dilatation, and found $r = \frac{2}{3}$. When this contribution is taken into account, r is closer to unity, as shown by Hayakawa, Smits & Bogdonoff (1984*b*). The analysis is based on rapid-distortion concepts, in that all turbulence/turbulence interactions are neglected, and that the turbulence distortion is due entirely to changes in the mean flow. At the level of this analysis, compression amplifies all stress components equally, and structure parameters such as a'' remain constant along streamlines.

To describe the evolution of the Reynolds-stress tensor more plausibly, Debieve *et al.* (1982) developed an analysis where the shock wave was modelled as a stationary discontinuity. The analysis takes into account the production by the mean-velocity gradients, and uses rapid-distortion concepts to describe the evolution of the other

		$\overline{u'^2}$	$\overline{v'^2}$	$\overline{w'^2}$	$\overline{q'^2}$	$-\overline{u'v'}$	$\frac{-\overline{u'v'}}{\overline{u'^2}}$	$\frac{-\overline{u'v'}}{\overline{q'^2}}$	$\frac{\langle u' \rangle}{\langle v' \rangle}$	$\frac{-\overline{u'v'}}{\langle u' \rangle \langle v' \rangle}$
upstream		1	0.40	0.66	2.06	0.32	0.32	0.155	1.58	0.27
8°	A	1.65	1.28	0.89	3.81	1.06	0.65	0.28	1.13	0.73
	B	1.63	1.43	0.91	3.97	1.11	0.68	0.28	1.07	0.73
	C	1.64	1.57	0.94	4.15	1.16	0.71	0.28	1.02	0.72
16°	A	2.95	3.53	1.17	7.64	2.74	0.93	0.36	0.91	0.85
	B	2.71	4.18	1.21	8.11	2.82	1.04	0.35	0.81	0.84
	C	2.68	4.88	1.27	8.83	3.00	1.12	0.34	0.74	0.83
20°	A	4.77	5.63	1.36	11.80	4.64	0.97	0.39	0.92	0.90
	B	3.64	6.63	1.38	11.60	4.30	1.18	0.37	0.74	0.88
	C	3.49	7.85	1.44	12.80	4.54	1.30	0.36	0.67	0.87

TABLE 2. Distortion of Reynolds-stress tensor according to the analysis of Debieve *et al.* (1982). A, B, C refer to streamlines shown in figure 1.

source terms. An algebraic relationship results, where the development of the Reynolds-stress tensor along a mean streamline depends only on its value in the upstream boundary layer, the shock strength, and the shock geometry defined by the unit normal vector.

Debieve *et al.* found encouraging agreement between the calculated and measured distortion of $\overline{u'^2}$ in a 6° compression corner at Mach 2.3. For the flows considered here, the results of the analysis are given in table 2. The elements of the upstream Reynolds-stress tensor that were not measured were assumed to be equal to generally accepted values, and the shock geometry and strength were found by assuming that all turning occurred across a single shock.

Large increases in all turbulence levels are predicted, particularly for $\overline{v'^2}$ and $\overline{u'v'}$, and the structure parameters are strongly distorted. For example, a'' is predicted to increase by factors of 2–4, and the anisotropy ratio $\langle u' \rangle / \langle v' \rangle$ is expected to decrease by factors of 1.4–2.4. Physically, this may be expected by considering the inviscid distortion of vortex filaments through the shock wave. Transverse filaments will be reduced in cross-sectional area by the ratio of the densities, longitudinal filaments will be reduced in cross-sectional area by the ratio of the mass-flow rates, and filaments normal to the wall will be reduced in cross-sectional area by the ratio of the velocities. Hence, all three components of vorticity are amplified but by different amounts. The strongest amplifications will be felt in the transverse and normal vorticity components, and both components contribute to v' fluctuations.

The comparison with experiment is rather variable. For the 20° corner, the analysis underpredicts the amplification of $\overline{u'^2}$ by factors of about 1.5–3.5 (see figure 10) but the predicted amplification of $\overline{u'v'}$ is much closer to experiment. For the 8° corner, all the predictions agree reasonably well with experiment. To explain these observations, we suggest that shock oscillation becomes more important at higher corner angles because the strength of the shock increases and eventually produces separation. The motion of the shock wave is a combination of bulk displacement, rotation and local deformation. Bulk displacement is 'externally driven', and for a compression-ramp geometry can be caused by unsteadiness in the incoming flow or when the position of the sonic line varies owing to upstream or downstream fluctuations in pressure. Rotation of the shock wave, that is to say a change in shock inclination,

can arise when the separated zone exhibits low-frequency 'breathing'. Local deformation is a result of the incoming turbulence. The difference between rotation and deformation depends on the relative amplitude and frequency of motion, and it is therefore somewhat arbitrary. Under the right circumstances, both types of distortion can propagate along the shock as a rippling motion and produce intense Reynolds stresses (Hussaini *et al.* 1985). If the shock movement is essentially random, we expect that the mean-flow energy is transferred more to the normal stresses rather than to the shear stresses. This explanation suggests that the motion of the shock wave generates significant 'inactive' motions such as those discussed by Bradshaw (1967) in relation to highly retarded subsonic boundary layers. Hence a'' will decrease in amplitude as the shock strength increases, as observed in the experiment.

To investigate the frequency content of the shock motion, Andreopoulos & Muck (1987) recently used conditional sampling to determine the probability distribution of the frequencies contained in the wall-pressure signal. They found that the distributions were highly skewed with long tails; the most probable values were close to 1 kHz, whereas the mean values were centred at about 8 kHz. Narlo (1986) has suggested that the conditional-sampling method used by Andreopoulos & Muck may have overestimated these frequencies, and that they may be significantly lower. Nevertheless, the spectra show considerable increase in energy content at frequencies near 1 kHz, and downstream of the interaction the frequency of the most energetic motions (f_e in figure 14) is near the mean shock-wave oscillation frequency found by Andreopoulos & Muck. More work is required but it is proposed that the shift to lower frequencies in the turbulence field, and the accompanying turbulence amplification is directly caused by the unsteady shock motion.

5. Conclusion

A rather complicated flow picture emerges. As the turbulent motions enter the interaction zone, they initially encounter a shock wave. The interaction of the shock wave with the incoming turbulence causes the shock to oscillate in the streamwise direction and wrinkle in the spanwise direction. If the shock is strong enough, separation occurs and the flow-field unsteadiness becomes increasingly important. As the turbulent motions pass through the shock, they are compressed and turned towards the shock, and this compression and turning continues for a considerable distance downstream. As a consequence of all these distorting influences, the turbulence activity greatly increases and the lengthscales are amplified.

All turbulent stresses show a qualitatively similar trend: they increase steeply on encountering the shock and the rate of increase is largest near the wall. The turbulence levels then decrease slowly under the action of redistribution and dissipation, and at the end of each model they are still decreasing. The maximum amplification of the r.m.s. quantities is approximately proportional to the overall static pressure rise through the interaction.

When the shock strength is relatively low, the turbulence amplification appears to be caused by direct, virtually inviscid amplification across the shock, followed by the combined effects of adverse pressure gradient, compressive extra strain rates and concave curvature. In this case, it seems that the important parameter is the overall pressure rise rather than the presence of a shock wave. This was recently confirmed by the results from the isentropic compression studies by Jayaram *et al.* (1987). When the shock strength increases, however, shock-wave oscillation becomes an important amplification mechanism. In these cases, mean flow energy is directly transferred into

unsteady turbulent motions. This process is apparently random, and therefore contributes more to the total turbulent energy than to the organized motions associated with the shear stresses. This hypothesis explains why the structure parameter a'' increases through the interaction for the 8° compression corner and decreases for the 16° and 20° compression corners; at the higher angles, shock-wave oscillation becomes important. Further support comes from an inspection of the spectra; the frequency content downstream of the interaction seems to strongly reflect the relatively low-frequency motion of the shock wave.

The experimental work was supported by NASA Headquarters Grant NAGW-240, monitored by Dr Gary Hicks. The analysis of the data and the preparation of this paper was supported by AFOSR Grant 85-0126, monitored by Dr James McMichael. Our thanks go to Margaret Taylor and Joseph Formica for preparing and plotting some of the figures.

REFERENCES

ADAMSON, T. C. & MESSITER, A. F. 1980 Analysis of two dimensional interactions between shock waves and boundary layers. *Ann. Rev. Fluid Mech.* **12**, 103–138.

AGRAWAL, S. & MESSITER, A. F. 1984 Turbulent boundary layer interaction with a shock wave at a compression corner. *J. Fluid Mech.* **143**, 23–46.

ANDREOPOULOS, J. & MUCK, K. C. 1987 Some new aspects of the shock wave boundary layer interaction in compression ramp flows. *J. Fluid Mech.* **180**, 405–428.

ANYIWO, J. C. & BUSHNELL, D. M. 1982 Turbulence amplification in shock wave/boundary layer interaction. *AIAA J.* **20**, 893–899.

ARDONCEAU, P., LEE, D. H., ALZIARY DE ROQUEFORT, T. & GOETHALS, R. 1979 Turbulence behavior in shock wave/boundary layer interaction. *AGARD CP-271, Paper* 8.

BRADSHAW, P. 1967 'Inactive' motion and pressure fluctuation in turbulent boundary layers. *J. Fluid Mech.* **30**, 241–258.

BRADSHAW, P. 1973 Streamline curvature effects in turbulent flow. *AGARDograph* 169.

BRADSHAW, P. 1974 The effect of mean compression or dilatation on the turbulence structure of supersonic boundary layers. *J. Fluid Mech.* **63**, 449–464.

COAKLEY, T. J., VIEGAS, J. R. & HORSTMAN, C. C. 1977 Evaluation of turbulence models for three primary types of shock-wave turbulence boundary layer interactions. *AIAA Paper* 77-692.

DEBIEVE, J. F., GOUIN, H. & GAVIGLIO, J. 1982 Evolution of the Reynolds stress tensor in a shock-turbulence interaction. *Indian J. Technol.* **20**, 90–97.

DOLLING, D. S. & MURPHY, M. 1982 Wall pressure in a supersonic separated compression ramp flow field. *AIAA Paper* 82-0986.

DOLLING, D. S. & OR, C. T. 1983 Unsteadiness of the shock wave structure in attached and separated compression ramp flow fields. *AIAA Paper* 83-1715.

DUSSAUGE, J. P. & GAVIGLIO, J. 1981 Bulk dilatation effects on Reynolds stress in the rapid expansion of a turbulent boundary layer at supersonic speed. In *Proc. Symp. Turbul. Shear Flows, Davis, CA*, vol. 2, pp. 33–38.

FERNHOLZ, H. H. & FINLEY, P. J. 1981 A further compilation of compressible boundary layer data with a survey of turbulence data. *AGARDograph* 263.

GREEN, J. E. 1970 Interactions between shock waves and turbulent boundary layers. *Prog. Aero. Sci.* **11**, 235–340.

HAYAKAWA, K., MUCK, K. C., SMITS, A. J. & BOGDONOFF, S. M. 1983 The evolution of turbulence in shock/wave boundary layer interactions. In *Proc. Eighth Australasian Fluid Mech. Conf.* Newcastle, Australia, pp. 9B7–9.

HAYAKAWA, K., SMITS, A. J. & BOGDONOFF, S. M. 1984*a* Hot-wire investigation of an unseparated shock wave/boundary layer interaction. *AIAA J.* **22**, 579–585.

HAYAKAWA, K., SMITS, A. J. & BOGDONOFF, S. M. 1984*b* Turbulence measurements in a compressible reattaching shear layer. *AIAA J.* **22**, 889–895.

HORSTMAN, C. C. & ROSE, W. C. 1975 Hot-wire anemometry in transonic flow. *NASA TMX*-62495.

HORSTMAN, C. C., SETTLES, G. S., VAS, I. E., BOGDONOFF, S. M. & HUNG, C. M. 1977 Reynolds number effects on shock-wave turbulent boundary layer interactions. *AIAA J.* **15**, 1152–1158.

HUSSAINI, M. Y., COLLIER, F. & BUSHNELL, D. M. 1985 Turbulence alteration due to shock motion. In *Proc. IUTAM Symp. Turbulent Shear-Layer/Shock-Wave Interactions, Palaiseau, France* (ed. J. Delery), pp. 371–382. Springer.

JAYARAM, M. & SMITS, A. J. 1985 The distortion of a supersonic turbulent boundary layer by bulk compression and streamline curvature. *AIAA Paper* 85-0299.

JAYARAM, M., TAYLOR, M. W. & SMITS, A. J. 1987 The response of a compressible turbulent boundary layer to short regions of concave surface curvature. *J. Fluid Mech.* **175**, 343–362.

KLINE, S. J., CANTWELL, B. J. & LILLEY, G. M. (eds) 1981 *Proc. 1980–81 AFOSR–HTTM Stanford Conf. Complex Turbul. Flow: Comparison of Computation and Experiment*, Vol. 1, Thermosci. Div., Stanford Univ., CA.

KOVASZNAY, L. S. G. 1980 The hot-wire anemometer in supersonic flow. *J. Aero. Sci.* **17**, 565–573.

KUSSOY, M. I. & HORSTMAN, C. C. 1975 An experimental documentation of a hypersonic shock-wave turbulent boundary layer interaction flow – with and without separation. *NASA TMX*-62412.

MORKOVIN, M. V. 1962 Effects of compressibility on turbulent flows. In *Mecanique de la Turbulence* (ed. A. Favre), pp. 367–380. Paris: CNRS.

MUCK, K. C., DUSSAUGE, J.-P. & BOGDONOFF, S. M. 1985 Structure of the wall pressure fluctuations in a shock-induced separated turbulent flow. *AIAA Paper* 85-0179.

MUCK, K. C., HAYAKAWA, K. & SMITS, A. J. 1983*a* Compilation of turbulence data for a 16 degree compression corner at Mach 2.9. *Princeton Univ., Dept of Mech. and Aero. Engng Rep.* 1619.

MUCK, K. C., HAYAKAWA, K. & SMITS, A. J. 1983*b* Compilation of turbulence data for a 20 degree compression corner at Mach 2.9. *Princeton Univ., Dept of Mech. and Aero. Engng Rep.* 1620.

MUCK, K. C. & SMITS, A. J. 1984*a* Behavior of a turbulent boundary layer subjected to a shock-induced separation. *AIAA Paper* 84-0097.

MUCK, K. C. & SMITS, A. J. 1984*b* The behavior of a compressible turbulent boundary layer under incipient separation conditions. In *Turbulent Shear Flows, IV*, pp. 235–45. Springer.

MUCK, K. C., SPINA, E. & SMITS, A. J. 1984 Compilation of turbulence data for an 8 degree compression corner at Mach 2.9. Normal and inclined wire data. *Princeton Univ., Dept of Mech and Aero. Engng Rep.* 1642.

NARLO, J. C. 1986 Experimental investigation of the driving mechanisms of separation shock wave motion in interactive flows. Ph.D. thesis, University of Texas, Austin, Texas, USA.

RONG, B. S., TAN, D. K. M. & SMITS, A. J. 1985 Calibration of the constant-temperature normal hot-wire anemometer in transonic flow. *Princeton Univ. Dept of Mech. and Aero. Engng Rep.* 1696.

ROSE, W. C. 1973 The behavior of a compressible turbulent boundary layer in a shock wave induced adverse pressure gradient. *NASA TN D*-7092.

ROSE, W. C. & MCDAID, E. P. 1977 Turbulence measurement in transonic flow. *AIAA J.* **15**, 1368.

ROSHKO, A. & THOMKE, G. J. 1966 Observations of turbulent reattachment behind an axisymmetric downstream-facing step in supersonic flow. *AIAA J.* **4**, 975–980.

SETTLES, G. S., FITZPATRICK, T. J. & BOGDONOFF, S. M. 1979 Detailed study of attached and separated compression corner flowfields in high Reynolds number supersonic flow. *AIAA J.* **17**, 579–585.

SHAMROTH, S. J. & MACDONALD, H. 1970 A new solution of the turbulent near wake recompression problem. *AIAA Paper* 70-0228.

SMITS, A. J., EATON, J. A. & BRADSHAW, P. 1979*a* The response of a turbulent boundary layer to lateral divergence. *J. Fluid Mech.* **94**, 243–268.

SMITS, A. J. & MUCK, K. C. 1984 Constant-temperature hot-wire anemometer practice in supersonic flows. Part II. The inclined wire. *Exp. Fluids* **2**, 33–41.

SMITS, A. J., MUCK, K. C. & HAYAKAWA, K. 1983 Constant-temperature hot-wire anemometer practice in supersonic flows. Part I. The normal wire. *Exp. Fluids* **1**, 83–92.

SMITS, A. J. & WOOD, D. H. 1985 The response of turbulent boundary layers to sudden perturbations. *Ann. Rev. Fluid Mech.* **17**, 321–358.

SMITS, A. J., YOUNG, S. T. B. & BRADSHAW, P. 1979*b* The effect of short regions of high surface curvature on turbulent boundary layers. *J. Fluid Mech.* **94**, 209–242.

TAYLOR, M. W. & SMITS, A. J. 1984 The effect of a short region of concave curvature on a supersonic turbulent boundary layer. *AIAA Paper* 84-0169.

TOWNSEND, A. A. 1976 *The Structure of Turbulent Shear Flow*, 2nd edn. Cambridge University Press.

VISBAL, M. & KNIGHT, D. D. 1983 Evaluation of the Baldwin–Lomax turbulence model for two-dimensional shock wave boundary layer interactions. *AIAA Paper* 83-1697.

ZANG, T. A., HUSSAINI, M. Y. & BUSHNELL, D. M. 1982 Numerical computations of turbulence amplification in shock wave interactions. *AIAA Paper* 82-0293.